15th International Symposium on Computer Methods in Biomechanics and Biomedical Engineering
and
3rd Conference on Imaging and Visualization
CMBBE 2018
P. R. Fernandes and J. M. Tavares (Editors)

EFFECT OF BIOFLUID RHEOLOGY AND WETTABILITY ON DROPLET DYNAMICS IN LAB-ON-CHIP SYSTEMS FOR CANCER DIAGNOSTICS

Frederico Jacinto[*], Ana S. Moita[†], António L.N. Moreira[†]

[*]IN+ - Center for Innovation, Technology and Policy Research, Dep. Mechanical Engineering,
Instituto Superior Técnico.
Av. Rovisco Pais, 1049-001 Lisboa, Portugal
frederico.jacinto@tecnico.ulisboa.pt

[†] IN+ - Center for Innovation, Technology and Policy Research, Dep. Mechanical Engineering,
Instituto Superior Técnico.
Av. Rovisco Pais, 1049-001 Lisboa, Portugal
anamoita@tecnico.ulisboa.pt; aluismoreira@tecnico.ulisboa.pt

Keywords: Lab-on-chip, Biofluids, Droplet Dynamics, Wettability, Numerical Model, Image post-processing.

Abstract: *This paper uses the dynamic behaviour of biofluid droplets under electrostatic actuation to identify relevant parameters for the design and test of a lab-on-chip device, based on microfluidic droplets, for cancer diagnostics. Chip configuration is designed inferring on the electrodes basic dimensions and positioning, depending on droplet's spreading/receding diameter and contact line velocity. These quantities are evaluated from post-processing procedures of images obtained combining high-speed visualization, time resolved infrared thermography and 3D Scanning Fluorescence Confocal Microscopy. The experimental results highlight the paramount role of the wetting properties of the dielectric coating covering the chips, which can strongly affect the spreading and the recoiling behaviour of the droplets, conditioning their motion and consequently the handling of the samples. Furthermore, an experimental evaluation, based on the decrease of the droplet contact diameter, height and local contact angle evidences a non-negligible occurrence of mass evaporation by diffusion from the droplet to the surrounding air, which requires control of the ambient conditions in the device, for ambient temperatures of the order of 20ºC or higher and relative humidity values below 80%. These experimental results agree well with the predictions from the numerical model devised and validated in the present work.*

1 INTRODUCTION

Biomicrofluidics and the fast development of lab-on-chip devices have opened a wide range of possibilities for sample manipulation and basic biochemical analysis, offering portability, flexibility, reduced use of samples and of reagents [1]. More recently, several studies in the literature report the development of lab-on-chips for future clinical diagnostics.

Such microfluidic devices are capable of performing blood samples separation, isolation of specific cells for further analysis, diagnostics based, for instance, on DNA analysis and cell sorting [2], but are not yet fully functional and validated for clinical use. Most of these devices are based on a microchannel configuration, which, despite being a validated working solution, still has some shortcomings, such as clogging and maintenance difficulties, lack of flexibility in the design and the requirement of auxiliaries such as pumps and valves, which have a very low efficiency at the microscale [3]. Alternatively, several authors stand for the use of microdroplets over open configuration chips, to transport and handle the samples. In this alternative configuration, an external actuation is required to assure a precise droplet motion in various manipulation operations. Different approaches have been studied such as for instance electromagnetic actuation or acoustic excitation [4], but electrowetting is still amongst the most popular solutions used. However, despite the well-based knowledge of the physics governing electrowetting, as reviewed in [5], there are still several issues which are not fully understood. For instance, the affinity of the dielectric material that covers the chips with the biosamples can be significant and affect droplet motion [6-7]. On the other hand, most of the studies addressing electrowetting applications on microchips, are mostly focused on the fundamentals and working principles, rather than on the device fabrication. However, the latter is strongly dependent on several parameters, such as the properties of the dielectrics and of the samples, which need to be accurately addressed in the design and test of the chips. Furthermore, for point-of-care applications, the chips must work under harsh environmental conditions without a very demanding control of temperature or relative humidity. Such conditions can promote the fast evaporation of the microdroplets by mass diffusion, which should be investigated and taken into account in the design, if the evaporation rate turns to be significant [7].

Hence, the present paper concerns the design and test of a simple lab-on-chip configuration, towards the development of a microfluidic device for clinical diagnostics. An experimental approach is followed to infer on the basic dimensions, allowing the best performance of the chip, evaluated based on droplet dynamics (spreading/receding diameter and contact line velocity). Then, to scale down this section for a proper integration in the device, these basic dimensions are introduced in a numerical model, used to optimize the distance between the electrodes, the thickness of the dielectric and the electric potential and frequency to be applied. A detailed study is performed to analyse the actual evaporation rate of the microdroplets under demanding environments and its impact on the performance of the lab-on-chips.

Droplet dynamics is used here for dimensioning purposes, but also as a first approach to look for relevant parameters which can be used as free label biomarkers for diagnostics. The basic idea for the diagnostic consists on the evaluation of cell deformability ratios, which are related to different stages of cell stiffness, which in turn can be potentially used for cancer diagnostics, following the work for instance reported by [8-9]. Besides this analysis, one will later infer on how the possible rheological variations caused by the different stages of cell stiffness can be correlated to droplet dynamics, being useful as a diagnostic tool.

2 MATERIALS AND METHODS

2.1 Experimental set-up and procedures

Test chips are made by arrays of interdigited coplanar electrodes printed on a 0.6 μm aluminium film by lithography and wet etch on a glass substrate with 102x45 mm^2 and 700

μm of width. A thin film of a dielectric material (*e.g.* PDMS – Polydimethylsiloxane, Teflon) was deposited on the chip assembly. Following some basic dimensioning, as reported by [10], different basic configurations were firstly attempted, where the width of the electrodes *w*, was varied between 120μm and 1400μm, for a fixed distance between them of 2*a*=60 μm.

The chips are actuated using DC current provided by a Sorensen DCR600-.75B power supply. The applied voltage was varied from 0 to 245 V. The frequency imposed for switching the polarities at the electrodes is programmed using a square wave, as in [11]. The imposed frequencies were varied between 0 and 400Hz.

Biofluid droplets of 1.5-5μL volume are deposited on the top of the chips which are then actuated under different working conditions.

All the experiments are performed in a Perspex chamber, saturated with the biofluid and under continuous monitoring of temperature and relative humidity of the surrounding air. Temperature and humidity measurements are taken with a DHT 22 Humidity & Temperature Sensor, at a sample rate of 0.5 Hz. Relative humidity is measured within 2-5% accuracy, while temperature measurements are obtained within ±0.5°C accuracy. The temperature was observed to be constant within T=20±3ºC and relative humidity was kept constant between 75% and 78%.

Given the importance of droplet dynamics in the future implementation of the diagnostic method, the performance of the chips is evaluated looking at the dynamic response of the droplets on the actuated chips. Several quantities such as the spreading diameter (diameter of the droplet as it spreads on the surface), the contact angles under actuation and the velocity of the contact line (derivative of the spreading diameter) are evaluated based on the post processing of high-speed images, taken at 2200 fps using a Phantom v4.2 from Vision Research Inc., with 512x512 pixels@2100fps resolution. For the present optical configuration, the spatial resolution is 25μm/pixel and the temporal resolution is 0.45 ms. The post-processing is performed using a home-made routine developed in Matlab. Temporal evolution of the contact (spreading and receding) diameters is presented as the average curve of at least 6 events (6 droplets), obtained under similar experimental conditions. So, 6 complete curves are considered for each voltage, frequency, electrode configuration, i.e. for all the parameters varied in the study. Then, maximum/averaged vales are taken to obtain the discrete values for the velocity and for D/D_0. Droplet diameter and droplet height were also measured for different conditions of air and of surrounding temperature and humidity, to evaluate the effect of mass diffusion in the droplet size, which naturally will affect the results.

Contact angle measurements are averaged from twelve events. Static and quasi-static angles are measured using an optical tensiometer (THETA, from Attention). For detailed characterization of the liquid-solid contact region and contact angle measurements with high spatial accuracy, an additional technique was used: the 3D Laser Scanning Fluorescence Confocal Microscopy 3D LSFCM, as described in detail in [12]. The measurements are performed with a laser with 552 nm wavelength, set for the power of 10.50 mW (3.00% of its maximum power) and gain of the photomultiplier (PMT) of 550V. These values were set after a sensitivity analysis on the contrast of the image (before the post-processing) and on the Signal to Noise Ratio (SNR). The images are recorded in the format 1024x1024 and the scanning frequency is 400 Hz. The z-step was fixed in 1μm for all the measurements. The pixel size achieved in this technique is, for the worse resolution 5.42μm, but can be as small as 500nm. A fluorescent dye - Rhodamine B (Sigma Aldrich) is used, which was chosen taken into account its excitation and emission wavelengths, to be compatible with the

wavelengths available in the Laser Scanning Confocal Microscope (Leica SP8), but also due to particular characteristics of the experimental conditions, in the present study. For the concentrations used here (0.0007936mg/ml<Concentration<0.496mg/ml) the physico-chemical properties of the working fluid are not altered by the presence of the dye. This technique is reported in detail in [12].

Surface and droplet temperatures are monitored using an infrared IR-high speed camera (ONCA-MWIR-InSb from Xenics - ONCA 4696 series), which is placed above the device. Configuration and calibration procedures are described in [13].

The biofluids used here are a solution of GFP – Green Fluorescent Protein, (produced and purified in house) with $1.71x10^{-3}$ mM concentration and GFP expressing *E. Coli* suspensions, with concentrations of $1x10^{9}$ cells/mL and $2x10^{9}$ cells/mL. The solutions were characterized in terms of density, surface tension and viscosity, as summarized in Table 1 and following the procedures described in [7] and in [14]. All the solutions depicted a Newtonian behaviour, from the rheological point of view, with a dynamic viscosity very close to that of water ($\mu=1x10^{-3}$ Ns/m^2).

Solution	Density ρ [kg/m^3]	Surface tension σ_{lv} [mN/m]
GFP ($1.71x10^{-3}$ mM)	998	72.2±0.7
E. Coli ($1x10^{9}$ cells/mL)	991	71.8±0.3
E. Coli ($2x10^{9}$ cells/mL)	982	61.3±0.2

Table 1: Physico-chemical properties of the GFP solution used in the present work.

Detailed description of the experimental method and procedures used is reported in [7,14].

2.2 Numerical method

The simulations were performed using COMSOL Multiphysics 4.3b. To evaluate the electric forces generated, the numerical domain considered was a 0.655mm radius sphere (droplet domain) within an air space of 3.21x1.6x3mm^3. The electrostatic boundary conditions are an electrical potential of 70V imposed to the electrode on the right (positive x-axis) and a ground (0V) imposed the electrode on the left [11]. The model considers a thin low permittivity gap with a 10μm dielectric layer [15]. The mesh is composed of 67025 tetrahedral elements, being refined at the liquid-solid and liquid-vapour interfaces.

For the simulation of droplet motion under transient conditions, the electrostatic boundary conditions are similar, but the distance between electrodes is imposed as $2a$ = 10μm, following the analysis of the electric force, as a function of this distance (as later discussed in the results). The numerical domain is a 0.655mm radius sphere (droplet domain) within an air space of 5X2mm^2. The mesh in this case is composed of 35831 free triangular elements, being also refined at the liquid-surface and liquid-air interfaces.

The electrostatic force actuating on the droplet is calculated using the Maxwell stress tensor, integrated on the droplet surface. A global evaluation method was used to perform

this integral in COMSOL. Hence, the electrostatic force is calculated by integrating:

$$n_1 T_2 = -\frac{1}{2} n_1 (E.D_e) + (n_1.E) {D_e}^T \tag{1}$$

on the surface of the droplet, where E is the electric field, D_e the electric displacement, and n_1 the outward normal from the object. Using the Maxwell stress tensor for a 2D configuration, the volume force is calculated as the first derivative of this tensor.

Regarding the droplet flow, Phase Field User Interface is used to track the liquid-air interface, for a laminar flow, using the incompressible formulation of the Navier-Stokes equations:

$$\rho \frac{\partial u}{\partial t} + \rho\,(u.\nabla) = \nabla.[-\mathrm{pI} + \mu(\nabla \mathrm{u} + \nabla u^T)] + F_g + F_a + F_{ext} + F \tag{2}$$

$$\nabla.\mathrm{u} = 0 \tag{3}$$

The four forces on the right-hand side of eq. (2) are due to gravity, surface tension, external contribution to the free energy, and a user defined volume force.

The phase field method adds the following equations:

$$\frac{\partial \Phi}{\partial t} + u.\nabla\Phi = \nabla.\frac{\gamma\lambda}{\varepsilon^2}\nabla\psi \tag{4}$$

$$\psi = -\nabla.\varepsilon^2\nabla\Phi + (\Phi^2 - 1)\Phi + \left(\frac{\varepsilon^2}{\lambda}\right)\frac{\partial f_{ext}}{\partial \Phi} \tag{5}$$

where the quantity λ (SI unit: N) is the mixing energy density and ε (SI unit: m) is a capillary width that scales with the thickness of the interface. These two parameters are related to the surface tension coefficient, σ (SI unit: N/m), through equation:

$$\sigma = \frac{2\sqrt{2}}{3}\frac{\lambda}{\sigma} \tag{6}$$

The volume fraction of air (fluid 2) is computed as:

$$V_f = \min(\max([1+f)/2],0,1) \tag{7}$$

where the min and max operators are used so that the volume fraction has a lower limit of 0 and an upper limit of 1. The density is then computed by:

$$\rho = \rho_1 + (\rho_2 - \rho_1)V_f \tag{8}$$

and the dynamic viscosity according to

$$\mu = \mu_1 + (\mu_2 - \mu_1)V_f \tag{9}$$

where ρ_1 and ρ_2 are the densities and μ_1 and μ_2 are the dynamic viscosities of fluid 1 (biofluids) and fluid 2 (air), respectively.

Since mass diffusion from the droplet to the surrounding air can be significant, to complement the experimental evaluation of the effect of mass diffusion on the size of the droplet, mass diffusion was included in the numerical model developed here, being evaluated using the diffusion-convection equation:

$$\frac{\partial c_i}{\partial t} + \nabla.(-D_i \nabla c_i) + u.\nabla c_i = 0 \tag{10}$$

which includes the transport mechanisms of diffusion and convection. Here c_i is the concentration of the species, D_i denotes the diffusion coefficient and **u** is the velocity vector.

The first term on the left-hand side of eq. (10) corresponds to the accumulation (or in this case consumption) of the species. The second term represents the diffusive transport, accounting for the interaction between the dilute species and the solvent.

The third term on the left-hand side of eq. (10) describes the convective transport, in the non-conservative formulation (incompressible fluid), due to a velocity field **u**. This term can be disregarded in the present work, given the very low velocity of the moving droplet.

The diffusion coefficient is $2.6 \times 10^{-5} m^2/s$, the initial water concentration in the surrounding air is 0.27688 mol/m³ (relative humidity of 0.29) and the droplet surface concentration is $ht.psat/(R_{const}.T)$, where ht.psat is the liquid enthalpy at the saturation pressure (for the temperature T), R_{const} is the ideal gases constant and T the temperature of the droplet. The boundary conditions consider no water flux for all the surfaces except for the droplet/air interfaces.

3 RESULTS AND DISCUSSION

3.1 Effect of the physico-chemical properties of the dielectric materials and of the biofluids

The microfluidic device to be developed should be composed by three main sections, namely i) the section transporting the microdroplets to the ii) diagnostics section and the final iii) sorting section. While the deformation of the cells is endorsed and studied in the diagnostics section, the precise control of droplets motion has a paramount role and therefore is the main focus at this early stage of development of the device. In this context, in recent

work, [7,14-16] showed that the project and design of the chip was strictly related to the wetting and electrochemical properties of the biofluids and of the dielectric materials covering the chips, as they strongly affect the motion of the deposited biofluids droplets. Vieira *et al.* [14] and Mata *et al.* [15] performed an extensive literature review on the most usual dielectric materials used in electrowetting chips and selected the most suitable materials, based on the dynamic response of the actuated biofluid droplets. Hence, the chosen materials should be repellent to the biofluid droplets (hydrophobic or superhydrophobic, i.e. depicting contact angles higher than 120º or 150º, respectively), to promote their spreading (allowing the droplets to easily touch consecutive electrodes) and should depict very low contact angle hysteresis (preferably lower than 11º), as the energy dissipated at the droplet-surface contact line is proportional to the hysteresis. Furthermore, [7,14,16] report the frequent adsorption of the biocomponents (mainly of the proteins) by most of the usual dielectric materials, which decreased locally the contact angle, promoting surface energy dissipation and restricting the motion of the droplet. Such effect is confirmed in the present study, as illustrated in Figure 1, which depicts the temporal evolution of the spreading diameters of GFP and *E-coli* suspension droplets ($1x10^9$ cells/mL), on a Teflon dielectric, for an applied voltage of 220V (similar behaviour is obtained within a wide range of voltages). t=0 s corresponds to the instant when the droplet is actuated. The curves obtained here are made non-dimensional with the initial contact diameter obtained for V=0 V - D_0, to account for small variations in the initial size of the droplet, which would be propagated along the entire temporal evolution. The effect of the concentration of the biocomponents in the microdroplets was consistently reported to be negligible in previous studies (*e.g.* [7,14]) so that only the most diluted solutions are used in the following analysis.

The figure shows that the spreading diameter of the droplets on the Teflon coated with Glaco© is considerably larger than that observed for the uncoated Teflon. The spreading is followed by a significant recoiling of the droplet, which is absent on the Teflon uncoated substrate. Glaco© is a perfluoroalkyltrichlorosilane combined with perfluoropolyether carboxylic acid and a fluorinated solvent [17] which turns the substrates superhydrophobic and reduces the protein adsorption, as shown in [7,14,16]. These effects combined, further reduce the contact angle hysteresis and, consequently, energy dissipation at the contact line, thus promoting droplet motion.

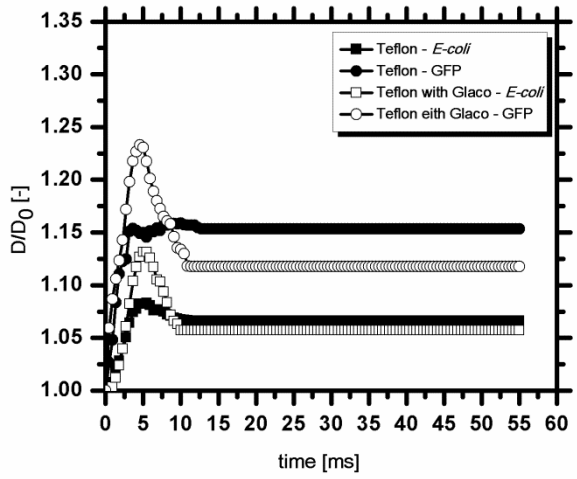

Figure 1: Temporal evolution of the spreading diameter for droplets of GFP and *E-coli* ($1x10^9$ cells/mL), actuated at 220V.

The reduced response to actuation of the droplet of *E. Coli* suspension is not perfectly clear yet, so that further work is required to understand this phenomenon. However, it is speculated that such reduced response can be related to a migration of the cells to the droplet-surface contact regions, which may affect the electric density and locally affect the surface wettability.

Following this preliminary analysis, the dielectric material covering the chips should be coated with Glaco©.

3.2 Optimization of the chip configuration

After selecting the dielectric material which will be in contact with the biofluid droplets, the configuration of the chip must be designed, defining the size and positioning of the electrodes. The motion of the droplet requires it to be in contact with at least two electrodes, which are actuated according to an imposed switching frequency. Following the recommendations of [10], four basic configurations were tested, varying the width of the electrodes, namely, w = 120μm, 800μm, 1200μm and 1400μm, with a fixed distance between electrodes, $2a$ = 60μm. However, while changing the width of the electrodes would not significantly alter the dynamic response of the actuated droplet [16], the experimental approach used was limiting the distance between the electrodes, which could not be optimized.

So, this distance was optimized using the numerical simulation, described in sub-section 2.2. The optimum distance between electrodes is the one maximizing the applied electric force, as shown in Figure 2.

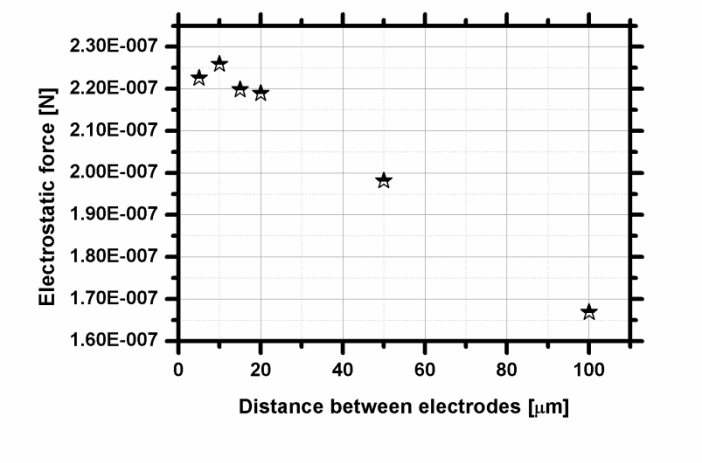

Figure 2: Electric force generated by the electrodes configuration, as a function of the distance between electrodes.

The numerical simulation considers as boundary conditions a contact angle matching the set PDMS+Glaco (θ_e = 153º) and a GFP droplet, with the properties shown in Table 1. The thickness of the film was reduced to 10μm, following the recommendations of [15,18].

Furthermore the entire simulation of the dynamic behaviour of the droplet for the optimum distance between electrodes *2a* = 10μm, (Figure 3) confirms a significant motion for an applied voltage of 70V, which is much lower than the 200V required in the first tested set of chips tested experimentally.

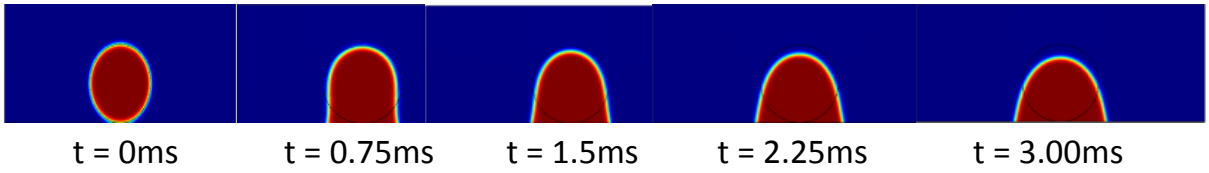

Figure 3: Sequence of images showing the motion of the GFP droplet on co-planar electrodes, spaced with a distance 2a = 10μm, for an imposed electric potential of 70V and an imposed frequency of 9Hz. The volume of the liquid droplet is 1.8μL.

These results, which are in qualitative agreement with those reported by [16] are quite encouraging, considering that other parameters such as the thickness of the dielectric layer are not optimized yet. Following these results, a new patch of chips is being currently produced to be further tested.

3.3 Evaporation effects and their impact of chip performance

The successful application of this kind of microfluidic devices in point-of-care diagnostics depends on how their performance is affected by the ambient conditions. In fact, as the biosamples are transported and manipulated in microdroplets, the ambient conditions should allow the microfluidic device to function without the occurrence of significant droplet evaporation. The temperature of the droplet $T_d(t)$ does not change during actuation, as shown in Figure 4, which depicts the maximum, minimum and average temperature of the droplet during actuation, taken with the infrared high-speed camera.

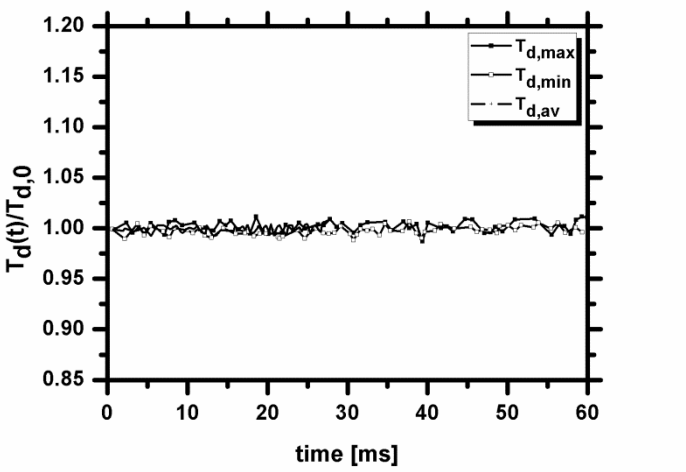

Figure 4: Maximum ($T_{d,max}$), minimum ($T_{d,min}$) and average ($T_{d,av}$) temperature values inside the droplet during electrostatic actuation at 220V.

The droplet temperature made dimensionless with the initial droplet temperature, before actuation $T_{d,0}$.

Hence, droplet evaporation should occur mainly by mass diffusion.

To evaluate the evaporation rate of the biofluid droplets, the temporal evolution of the droplets angle, spreading diameter and height was measured for specific ambient (temperature and relative humidity) conditions, monitored with the DHT 22 Humidity & Temperature Sensor. The temporal evolution of the angles, diameter and height of the biofluid droplets was evaluated after post-processing the images taken by 3D Laser Scanning Fluorescence Confocal Microscopy. The droplets are evaluated in two planes, XZ and YZ, respectively, to detect possible asymmetries in the processes under study (Figure 5a).

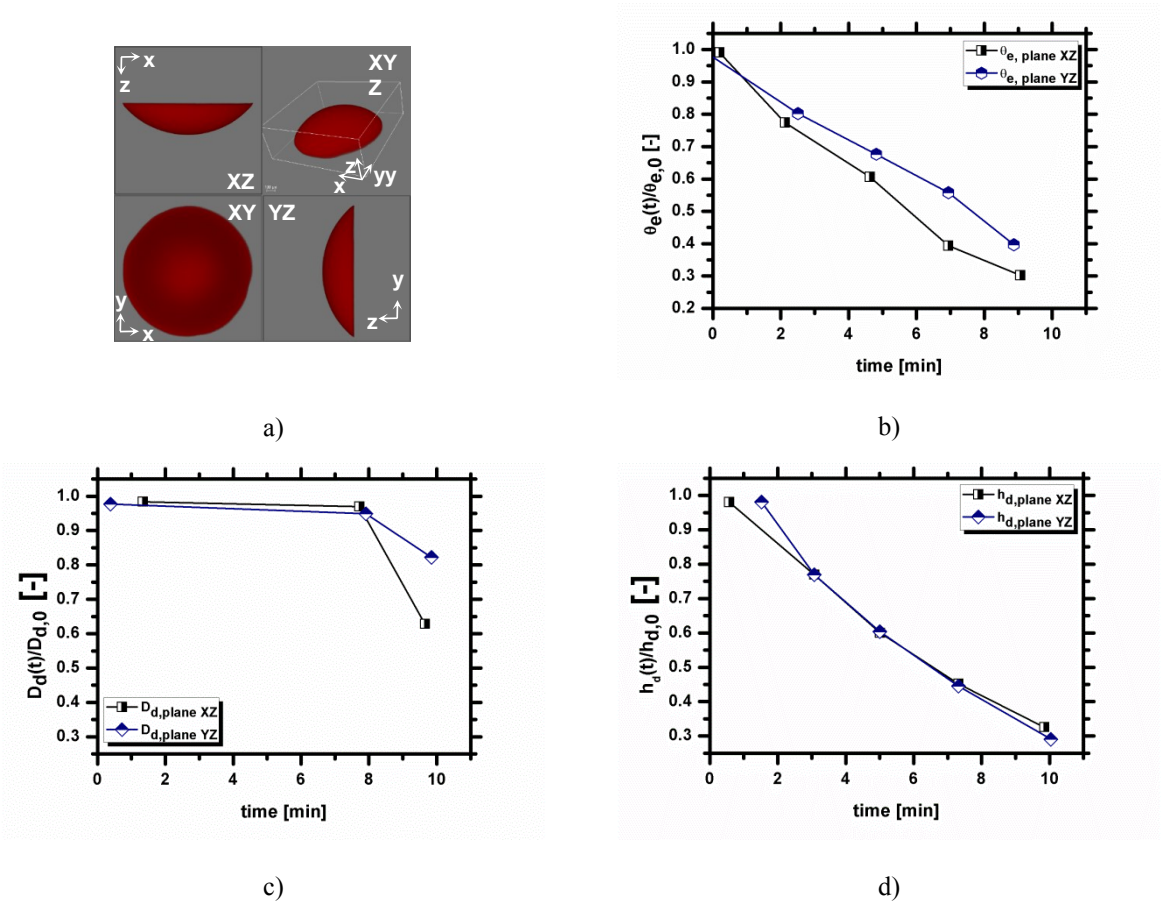

Figure 5: Evaluation of droplet evaporation by mass diffusion. a) Definition of planes XZ and YZ. b) Temporal evolution of the equilibrium contact angle θ_e made non-dimensional with the initial contact angle of the deposited droplet $\theta_{e,0}$, c) Temporal evolution of droplet spreading diameter $D_d(t)$ and d) height $h_d(t)$ for the planes XZ and YZ of the droplet profile. $D_{d,0}$ and $h_{d,0}$ stand for the initial diameter and height of the deposited droplet, respectively. The ambient temperature is 20ºC±2ºC and the relative humidity is 88.5%.

The relative humidity is gradually decreased and for values of the order of 88% the equilibrium contact angle θ_e decreases linearly 68% and 60% the XZ and YZ planes, respectively (Figure 5b) in comparison to the initial value measured at the deposited droplet $\theta_{e,0}$. The diameter decreases 36% (plane XZ) and 17% (plane YZ) in comparison to the initial state (Figure 5c) and the droplet height decreases linearly by roughly 67% of its initial value,

for both planes (Figure 5d). These quantities were evaluated over a time span of 10 min.

These experimental results confirm the theoretical analysis reported in [7] who predict an evaporation rate by mass diffusion up to 30%, for time intervals of 1500s within a relative humidity of 70%. These results are also in agreement with those obtained in our model.

Hence, following this analysis, one should recommend a mild control of the ambient conditions in these devices, while keeping them as simple as possible, to minimize this evaporative effect.

4 CONCLUSIONS

The present paper addresses the study of the dynamic behaviour of biofluid droplets under electrowetting, towards the development of a microfluidic (lab-on-chip) device, to be used in the near future in cancer diagnostics. At this stage of the work, we describe the design and test of the microfluidic device. Hence post-processing procedures of the images taken by combining high-speed visualization with infrared high-speed thermography and with 3D Laser Scanning Fluorescence Confocal Microscopy are used to evaluate quantitatively the spreading and receding diameter, droplet height and contact line velocity (velocity of displacement) of the droplets under electrostatic actuation. These quantities are then used to optimize the configuration (size and position) of the electrodes and to select the most appropriate materials. The experimental results show that the wetting properties of the dielectric material that covers the chips must be chosen in order to minimize the energy dissipation at the droplet-surface contact line. This will assure the proper droplet motion, thus allowing the precise handling of the biosamples. Furthermore, evaluating the temporal evolution of these quantities on the droplet allowed to monitor changes in droplet volume associated to mass evaporation by diffusion. The analysis performed shows a non-negligible mass evaporation by diffusion, for ambient temperatures above 20ºC and relative humidity below 80%, which must be taken into account in the fabrication of the device. These results are in good agreement with theoretical analyses reported in the literature and with the numerical model that was developed and validated in the present work.

ACKNOWLEDGEMENTS

The authors are grateful to Fundação para a Ciência e Tecnologia (FCT) for financing Ana S. Moita's contract and exploratory research project through the recruitment programme FCT Investigator (IF 00810-2015).

REFERENCES

[1] A.R. Wheeler, H. Moon, C.J. Kim, J.A. Loo. Electrowetting-based microfluidics for analysis of peptides and proteins by matrix-assisted laser desorption/ionization mass spectrometry, *Analytical Chemistry*, **76**, 4833–4838, 2004.

[2] A. Dance. The making of a medical microchip. *Nature*, 545, 512-514. 2017.

[3] H. Geng, J. Feng, L.M. Stabryl, S.K. Cho. Dielectrowetting manipulation for digital microfluidics: creating, transporting, splitting, and merging droplets. *Lab-on-Chip*, **17**, 1060-1068. 2017.

[4] J. Bennès, S. Alzuaga, F. Chérioux, S. Ballandras, P. Vairac, J.-F. Manceau, F. Bastien. Detection and high-precision positioning of liquid droplets using saw systems, IEEE Transactions on ultrasonics, ferroelectrics and frequency control, 54(10), 2007.

[5] W. C. Nelson, C.-j. Kim. Droplet actuation by Electrowetting-on-Dielectric (EWOD): A review. *J. Adhesion Sci. Tech.*, **26**, 1747-1771, 2012.

[6] J.Y. Yoon, R.L. Garrell. Preventing biomolecular adsorption in electrowetting-based biofluidic chips, *Analytical Chemistry*, **75**, 5097–5102, 2003.

[7] A.S. Moita, C. Laurência, J.A. Ramos, D.M.F. Prazeres, A.L.N. Moreira. Dynamics of droplets of biological fluids on smooth superhydrophobic surfaces under electrostatic actuation, *J. Bionic Eng.*, **13**, 220-234, 2016.

[8] G.R. Gosset, H.T.K. Tse, S.A. Lee, Y. Ying, A.G. Lidgren, O.O. Yang, J. Rao, A.T. Clark, D. Di Carlo. Hydrodynamic stretching of single cells for large population mechanical phenotyping, PNAS, **109**(20), 7630-7635, 2010.

[9] S.E. Cross, Y.-S. Jin, J. Rao, J.K. Gimzewski. Nanomechanical analysis of cells from cancer patients. *Nature Nanotechnology Letters*, **2**, 780-783, 2005.

[10] J.Z. Chen, A.A. Darhuber, S.M. Troian, S. Wagner. Capacitive sensing of droplets for microfluidic devices based on thermocapillary actuation, *Lab-on-a-Chip*, **4**(5), 473–480, 2004.

[11] S.-K. Fan, H. Yang, T.-T. Wang, W. Hsu. Asymmetric electrowetting-moving droplets by a square wave. *Lab-on-a-Chip*, **7**(10), 1330–1335, 2007.

[12] D. Vieira, A.S. Moita, A.L.N. Moreira. Non-intrusive wettability characterization on complex surfaces using 3D Laser Scanning Confocal Fluorescence Microscopy, *18th International Symposium on Applications of Laser and Imaging Techniques to Fluid Mechanics, Lisbon*, 2016.

[13] P. Pontes, E. Teodori, A.S. Moita, A.L.N. Moreira. Thermographic analysis of interfacial heat transfer mechanisms with high temporal resolution. *9th World Conference on Experimental Heat Transfer, Fluid Mechanics and Thermodynamics, ExHFT-9, 12-15 June, Iguazu Falls, Brazil*, 2017.

[14] D. Vieira, F. Mata, A.S. Moita, A.L.N. Moreira. Microfluidic Prototype of a Lab-on-Chip Device for Lung Cancer Diagnostics. *Proceedings of the 10th International Joint Conference on Biomedical Engineering Systems and Technologies - Volume 1: BIODEVICES*, 63-68, 2017, Porto, Portugal, 21-13 February 2017. DOI: 10.5220/0006252700630068, ISBN: 978-989-758-216-5,1017.

[15] F. Mata, A.S. Moita, R. Kumar, S. Cardoso, D.M.F. Prazeres, A.L.N. Moreira. Effect of surface wettability on the spreading and displacement of biofluid drops in electrowetting. *Proceedings of ILASS – Europe 2016, 27th Annual Conference on Liquid Atomization and Spray Systems, Sep. 2016, Brighton, UK 4-7 September 2016. ISBN 978-1-910172-09-4*, 2016.

[16] F. Jacinto, A.S. Moita, A.L.N. Moreira. Design, test and fabrication of a droplet based microfluidic device for clinical diagnostics. *Proceedings of the 11th International Conference on Biomedical Electronics and Devices – Volume 1: BIODEVICES 2018, 19 – 21 January, Funchal, Madeira*, 88-95. ISBN 978-989-758-277-6, 2018.

[17] M. Kato, A. Tanaka, M. Sasagawa, H. Adachi. Durable automotive windshield coating and the use thereof. US Patent, 8043421 B2, 2008.

[18] V. Di Virgilio. Contactless electrowetting, PhD Thesis, Universitat Politècnica de Catalunya, Catalunya, Spain, 2015.